Accepted Manuscript

Effects of La doping on structural, optical, electronic properties of $Sr_2Bi_2O_5$ photocatalyst

Yuki Obukuro, Shigenori Matsushima, Kenji Obata, Takuya Suzuki, Masao Arai, Eiji Asato, Yuji Okuyama, Naoki Matsunaga, Go Sakai

PII: S0925-8388(15)31455-9

DOI: 10.1016/j.jallcom.2015.10.199

Reference: JALCOM 35754

To appear in: *Journal of Alloys and Compounds*

Received Date: 22 June 2015

Revised Date: 19 October 2015

Accepted Date: 21 October 2015

Please cite this article as: Y. Obukuro, S. Matsushima, K. Obata, T. Suzuki, M. Arai, E. Asato, Y. Okuyama, N. Matsunaga, G. Sakai, Effects of La doping on structural, optical, electronic properties of $Sr_2Bi_2O_5$ photocatalyst, *Journal of Alloys and Compounds* (2015), doi: 10.1016/j.jallcom.2015.10.199.

Graphical abstract

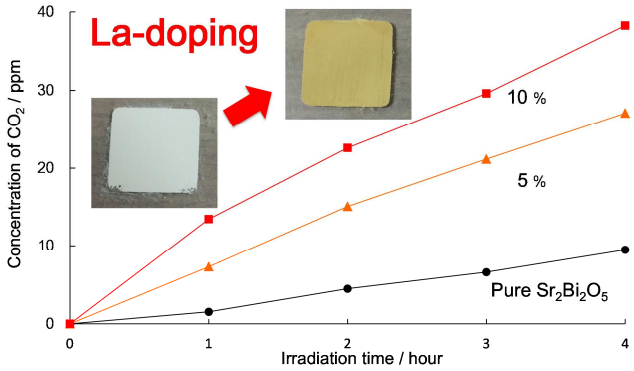

Effects of La doping on structural, optical, electronic properties of $Sr_2Bi_2O_5$ photocatalyst

Yuki Obukuro [a], Shigenori Matsushima [b,*], Kenji Obata [b], Takuya Suzuki [c], Masao Arai [d], Eiji Asato [e], Yuji Okuyama [f], Naoki Matsunaga [g] , Go Sakai [g,*]

[a]*Interdisciplinary Graduate School of Agriculture and Engineering, University of Miyazaki, 1-1 Gakuenkibanadai-nishi, Miyazaki 889-2192, Japan*

[b]*Department of Creative Engineering, National Institute of Technology (NIT), Kitakyushu College 5-20-1 Shii, Kokuraminami-ku, Kitakyushu 802-0985, Japan*

[c]*Graduate School of Environmental Engineering, The University of Kitakyushu, Hibikino, Wakamatsu-ku, Kitakyushu 808-0135, Japan*

[d]*Computational Materials Science Unit (CMSU), National Institute of Materials Science (NIMS), 1-1 Namiki, Tsukuba 305-0044, Japan*

[e]*Department of Chemistry, Biology and Marine Science, University of the Ryukyus, 1 Senbaru, Nishihara-cho, Okinawa 903-0213, Japan*

[f]*Organization for Promotion of Tenure Track, University of Miyazaki, 1-1 Gakuenkibanadai-nishi, Miyazaki 889-2192, Japan*

[g]*Department of Environmental Robotics, Faculty of Engineering, University of Miyazaki, 1-1 Gakuenkibanadai-nishi, Miyazaki 889-2192, Japan*

(Received 17 June 2015; Revised)

*Corresponding authors

Tel: +81-93-964-7309; Fax: +81-93-964-7309; E-mail: smatsu@kct.ac.jp

Tel: +81-985-58-7312; Fax: +81-985-58-7312; E-mail: sakai-go@cc.miyazaki-u.ac.jp

Abstract

Single-phase $Sr_2Bi_2O_5$ was obtained by calcination of the heterobimetallic complex precursor Sr[Bi(DTPA)]•$9H_2O$ (DTPA is diethylenetriaminepentaacetic acid) at 700 °C for 6 h. The effect of La doping on the crystal structure, surface area, morphology, surface chemical state, and absorption properties of $Sr_2Bi_2O_5$ samples prepared from Sr[Bi(DTPA)]•$9H_2O$ were investigated. No traces of an impurity phase were detected in samples with a lower La content (3 and 5 mol%), while impurity phases such as $Sr_6Bi_2O_9$ and $SrCO_3$ were observed in $Sr_2Bi_2O_5$ samples with larger La contents of 8 and 10 mol%. The Brunauer–Emmett–Teller surface area of $Sr_2Bi_2O_5$ increased slightly with the content of La. High-resolution transmission electron microscopy revealed clear crystalline planes for both undoped and La-doped $Sr_2Bi_2O_5$ samples without amorphous phases. Meanwhile, X-ray photoelectron spectroscopy indicated that the valence states of constituent metals were Sr^{2+}, Bi^{3+}, and La^{3+}. The solubility limit of La in the $Sr_2Bi_2O_5$ crystal phase was determined from Raman scattering measurements. La atoms substituted Bi sites when the doping content was low, while both Bi and Sr sites were substituted with La when the content of La was high. The electronic structure of $Sr_2Bi_2O_5$ could be modified by La doping, resulting in a red shift of the absorption edge with increasing La content. The band-gap narrowing of $Sr_2Bi_2O_5$ with La-doping was reproduced in energy-band calculations. The photocatalytic activity of $Sr_2Bi_2O_5$ under visible-light irradiation for the oxidation of isopropanol was enhanced by doping with La.

Keyword: Heterobimetallic complex, La-doped $Sr_2Bi_2O_5$, Raman spectroscopy, Optical spectroscopy, Photocatalysis, Electronic band structure

1. Introduction

Since the discovery that Bi-Sr(-Ca)-Cu-O is a superconductor with high Curie temperature, the unique characteristics of SrO-Bi_2O_3 complex oxides have attracted considerable attention [1]. In the SrO-Bi_2O_3 system, stoichiometric complex oxides including $SrBi_2O_4$, $Sr_2Bi_2O_5$, $Sr_3Bi_2O_6$, $Sr_6Bi_4O_{15}$, $Sr_6Bi_2O_{11}$, and $Sr_{24}Bi_{14}O_{52}$ have been reported and the properties of these oxides depend on their chemical composition [2]. Among these SrO-Bi_2O_3 complex oxides, $Sr_2Bi_2O_5$ has recently received much interest as a photocatalyst material because of its fairly high photocatalytic activity [3,4].

The extensive hydrolysis of Bi(III) species in water leads to deviation of the chemical formula of the final product from the starting molar ratio when SrO-Bi_2O_3 complex oxides are synthesized by wet processes [5]. Thus, SrO-Bi_2O_3 complex oxides are typically prepared by solid-state reaction. However, solid-state reactions still face some problems, such as difficulty controlling crystal growth, the formation of impurity phases, and harsh calcination conditions [6]. From the viewpoint of practical application as a photocatalyst, the low surface area of the final products obtained by conventional solid-state reaction is one of its most severe disadvantages. This is because the photocatalytic activity of a material strongly depends on its surface area. In the SrO-Bi_2O_3 system, calcination at a high temperature for a long period is needed for grain growth, resulting in a low surface area. In contrast, when the molar ratio of Sr to Bi can be maintained during hydrolysis in wet processes, the grain size of the resulting SrO-Bi_2O_3 complex oxides can be easily controlled. It is known that several polydentate chelators classified as polyamino-polycarboxylate systems, such as ethylenediaminetetraacetic acid, diethylenetriaminepentaacetic acid (H_5DTPA), nitrilotriacetic acid, and *N*-(2-hydroxyethyl)iminodiacetic acid, are capable of forming stable 1:1 Bi:ligand complexes even in water. These complexes are suitable for producing precursors to obtain the objective photocatalyst materials following calcination.

Recently, our group reported that single-phase $Sr_2Bi_2O_5$ was formed by calcination of the heterobimetallic complex Sr[Bi(DTPA)]•9H_2O [7]. Furthermore, a preliminary test revealed that La-doping is effective to improve the photocatalytic activity of the single-phase $Sr_2Bi_2O_5$ for oxidation of isopropanol under visible-light irradiation. It has been reported that the high photocatalytic activity of $Sr_2Bi_2O_5$ can be attributed to the

effective separation of photogenerated electron–hole pairs originating from the distorted local structure of [BiO_6] polyhedra and their consequent dipole moment [3,4,8]. Additionally, a first-principles energy band calculation indicated that $Sr_2Bi_2O_5$ has light effective masses of photogenerated carriers because of its wide band dispersion near the valence-band (VB) maximum and conduction-band (CB) minimum [9,10]. This calculation also suggests that the photoactivity of $Sr_2Bi_2O_5$ could be enhanced by controlling its energy band structure and band gap. In our previous report, La was selected as a trivalent lanthanoid to maintain the distorted local structure of [BiO_6] polyhedra, and we found that doping with La led to $Sr_2Bi_2O_5$ with the band-gap narrowing [7].

In the present study, we thoroughly investigate the preparation conditions of La-doped and undoped $Sr_2Bi_2O_5$ powders, and the physicochemical properties of the products by analytical measurements such as X-ray diffraction (XRD), X-ray fluorescence analysis (XRF), X-ray photoelectron spectroscopy (XPS), Raman scattering spectroscopy, scanning electron microscopy (SEM), transmission electron microscopy (TEM), ultraviolet-visible (UV-vis) spectroscopy, and N_2 adsorption/desorption measurements, as well as examining the effect of La doping on the photocatalytic activity of the material. In addition, theoretical calculations of undoped and La-doped $Sr_2Bi_2O_5$ are conducted to elucidate the photoabsorption properties of the final products as well as the relationships between their electronic structure and photocatalytic activity.

2. Experimental and calculation procedures

2.1. Synthesis of undoped and La-doped $Sr_2Bi_2O_5$

Bismuth subcarbonate ($(BiO)_2CO_3$; 97.0%) was added to an aqueous solution of H_5DTPA (98.0%) (reaction 1). The resulting solution of [$Bi(H_2DTPA)$] was then reacted with an equivalent amount of $Sr(OH)_2{\cdot}8H_2O$ (95.0%) to obtain a solution of Sr[Bi(DTPA)] (reaction 2).

$$(BiO)_2CO_3 + 2H_5DTPA \rightarrow 2[Bi(H_2DTPA)] + 3H_2O + CO_2 \qquad \text{(reaction 1)}$$

$$[Bi(H_2DTPA)] + Sr(OH)_2 \rightarrow Sr[Bi(DTPA)] + 2H_2O \qquad \text{(reaction 2)}$$

After the removal of a trace amount of insoluble material by filtration, the filtrate was concentrated to dryness using a rotary evaporator. The obtained amorphous solid was

identified as $Sr[Bi(DTPA)]\bullet 9H_2O$ based on elemental analysis of C, H, and N atoms (Microcorder JM10, J-Science), thermogravimetric (TG) analysis (Thermo plus EVOII TG8120, Rigaku), and infrared (IR) spectroscopy (FTS3000, Excalibur). The amorphous solid was heated at 500 to 700 °C for 6 h in air. The heating rate was 10 °C/min in all cases. La was doped into $Sr[Bi(DTPA)]\bullet 9H_2O$ using $La_2(CO_3)_3\bullet nH_2O$ (99.5%), which was dissolved in the $[Bi(H_2DTPA)]$ solution before $Sr(OH)_2$ addition. La-doped $Sr_2Bi_2O_5$ ($Sr_2Bi_{2-x}La_xO_5$) samples with La doping contents of 3, 5, 8 and 10 mol% on the basis of Bi atoms (x = 0.06, 0.10, 0.16 and 0.20) were prepared.

2.2. Characterization of the precursor and final products

The thermal decomposition of DTPA complexes was analyzed by thermogravimetric-differential thermal analysis (TG-DTA; TG8120, Rigaku) under static atmosphere. XRD measurements were conducted to analyze the crystal structure of the calcined powders (Ultima IV, Rigaku). XRD patterns were recorded with Cu-Kα radiation at a sweep rate of 2 °/min, voltage of 30 kV and current of 20 mA. The specific surface areas of powders were evaluated from N_2 adsorption isotherms measured at –196 °C using the Brunauer–Emmett–Teller (BET) method in the relative pressure range of $0.1 < p/p_0 < 0.3$ by a surface area analyzer (BELSORP-mini II, BEL Japan, Inc.) [11,12]. The chemical composition and valence state of the precursors and final products were verified using XRF (EDXL 300, Rigaku) and XPS (JPS-9010MX, JEOL) measurements, respectively. The microstructure of the products was observed by SEM (S-5200, Hitachi, Ltd.) and TEM/HRTEM (JEM-3010, JEOL). Raman spectra were recorded on a Raman spectrometer (inVia Raman microscope, Renishaw) equipped with a CCD detector at room temperature using a 532-nm semiconductor laser and laser power <1.5 mW. Diffuse reflectance spectra (DRS) were collected using a UV-vis spectrometer (V-550, JASCO) over the wavelength range of 300 to 800 nm at room temperature.

2.3. Photocatalytic activity

The photocatalytic properties of undoped and La-doped $Sr_2Bi_2O_5$ were evaluated by their ability to completely oxidize isopropanol under visible-light irradiation. Each powder (50 mg) was uniformly dispersed on a glass substrate that was mounted in a

1.0-L cylindrical glass reactor equipped with a quartz window. After filling the reaction vessel with dry air (80% N_2, 20% O_2), isopropanol (100 μL) was introduced into the reactor using a syringe and then vaporized by keeping the vessel at 50 °C for 8 h. The optical system consisted of a 500-W Xe arc lamp and cut-off filter ($\lambda \geq 420$ nm). The irradiation power density was kept at 100 mW/cm^2. Photocatalytic activities were evaluated by the amount of CO_2 produced from the oxidation of isopropanol after visible-light irradiation for 4 h using a gas chromatograph equipped with a thermal conductivity detector.

2.4. Theoretical calculation

$Sr_2Bi_2O_5$ crystallizes as an orthorhombic structure in space group *Pnma* and contains four formula units in its unit cell to give a total of 36 atoms [13]. Bi and Sr atoms occupy the Wyckoff 4c position, while O atoms occupy the Wyckoff 4c and 8d positions. In this structure, there are two independent Sr atoms (Sr1 and Sr2), two independent Bi atoms (Bi1 and Bi2), and three independent O atoms (O1, O2 and O3). In the present calculation, two La-doped supercells, type 1 and type 2, were constructed in which a Bi1 or Bi2 atom, respectively, was substituted by a La atom in the expanded $Sr_2Bi_2O_5$ 2 × 2 × 1 cell (Fig. 1). The expanded $Sr_2Bi_2O_5$ 2 × 2 × 1 cell was in space group *Pm* and contained 144 atoms. In the supercell, there were 24 independent Sr atoms (Sr1 to Sr24), 23 independent Bi atoms (Bi1 to Bi23), and 44 independent O atoms (O1 to O44) in addition to one La atom. The type 1 and type 2 supercells were optimized by relaxing all of the atomic positions using the CASTEP code [14]. Lattice constants *a*, *b*, and *c* were assumed to have the same values as those in the expanded $Sr_2Bi_2O_5$ cell. The exchange and correlation interactions were treated within the framework of the generalized gradient approximation (GGA) proposed by Perdew, Burke, and Ernzerhof (PBE) [15]. The cutoff energy of the plane-wave expansions was set at 610 eV. Valence electrons were treated with Vanderbilt-type nonlocal ultrasoft pseudopotentials, which describe the effective potentials of ions and tightly bound core electrons [16]. The reciprocal-space integration was performed with two irreducible k points, which corresponded to a 1 × 2 × 3 k-point grid [17]. The electronic structure calculations for the type 1 and type 2 supercells were performed using the scalar-relativistic full potential linearized augmented plane wave (FLAPW) method [18].

The wave functions were expanded by APW basis functions composed of plane waves in the interstitial region and linear combinations of radial functions multiplied by spherical harmonics inside the muffin-tin (MT) region. The MT sphere radii (R_{MT}) of the La, Sr, Bi, and O atoms were 1.97, 1.83, 2.06, and 1.74 a.u., respectively. The plane-wave cutoff was $R_{MT} \times K_{max} = 6.0$, which produced 12,355 plane waves for the La-doped $Sr_2Bi_2O_5$ supercell. Each self-consistency was judged from the convergence criteria of charge, total energy, and force. We also verified the sensitivity of the total energy to the number of k points in each self-consistent calculation and observed a total energy decrease of only 0.26 mRy/atom for $R_{MT} \times K_{max} = 6.0$ when the number of k points increased from 27 to 68. Therefore, we concluded that the total energy was convergent for k points and used 27 k points for the Brillouin-zone (BZ) integration. In density of states (DOS) calculations, BZ integration was performed using the modified tetrahedron method on a special mesh of 27 k points.

3. Results and discussion

3.1. IR and TG-DTA analysis of the precursor

It is well known that H_5DTPA forms a heterobimetallic complex of Sr[Bi(DTPA)] upon mixing with Bi and Sr ions, as shown inreaction 1 and 2 above. The hydration of the heterobimetallic complex precursor determined by elemental and TG analyses was Sr[Bi(DTPA)]•$9H_2O$. IR spectra of H_5DTPA and Sr[Bi(DTPA)]•$9H_2O$ are depicted in Fig. 2. For H_5DTPA, the ν(C=O) stretches of -COOH groups were observed at approximately 1690 cm^{-1}. These stretching bands shifted to a doublet at approximately 1380 and 1600 cm^{-1} for Sr[Bi(DTPA)]·$9H_2O$, indicating the -COOH groups of DTPA were deprotonated by metal coordination to form chelates [19]. There were also large differences in peaks from -OH groups around 3,600 to 3,000 cm^{-1} between the anhydrous H_5DTPA and hydrated heterobimetallic complex Sr[Bi(DTPA)]•$9H_2O$. These differences were simply caused by the presence or absence of water molecules. No other notable differences were observed, so the obtained precursor was judged to be the objective heterobimetallic complex.

Figure 3 depicts the TG-DTA results for Sr[Bi(DTPA)]•$9H_2O$ measured at a heating rate of 10 °C/min. Dehydration started at approximately 50 °C and a plateau was observed over the temperature range of 185 to 300 °C. The weight decrease at 185 °C

was approximately 16.5 wt%, and was attributed to the desorption of water from Sr[Bi(DTPA)]•$9H_2O$. Further heating caused a weight loss originating from the exothermal decomposition of a ligand, as confirmed by DTA measurements. When Sr[Bi(DTPA)]•$9H_2O$ was heated to 750 °C, a long plateau appeared from 429 to 575 °C, followed by a slight decrease in weight. The weight loss at 700 °C was approximately 56.0 wt%. Based on these assignments, the following two-step decomposition mechanism can be proposed:

$$Sr[Bi(DTPA)]\bullet 9H_2O \rightarrow Sr[Bi(DTPA)] + 9H_2O \qquad \text{(reaction 3)}$$

$$4Sr[Bi(DTPA)] + 81O_2 \rightarrow 2Sr_2Bi_2O_5 + 28CO_2 + 6NO_2 + 18H_2O \qquad \text{(reaction 4)}$$

The theoretical weight losses for reaction 3 and 4 are calculated to be 18.9% and 58.9%, respectively, which agree well with the experimental values obtained from TG-DTA.

3.2. XRD and BET analyses of the calcined powders

Figure 4(a) presents the XRD patterns of the final products obtained following calcination of Sr[Bi(DTPA)]•$9H_2O$ at 500, 600, 650 and 700 °C for 6 h in air. The diffraction peaks of the samples calcined at 500, 600 and 650 °C can be ascribed to $SrBi_4O_7$ (PDF 00-046-0752), $Sr_2Bi_6O_{11}$ (PDF 00-049-1593), $SrBi_2O_4$ (PDF 00-039-1424), and $SrCO_3$ (PDF 01-071-2393) indicating that these calcination temperatures were too low to form objective material. In contrast, these impurity peaks completely vanished and a single phase of $Sr_2Bi_2O_5$ (PDF 01-081-0516) appeared following calcination of Sr[Bi(DTPA)]•$9H_2O$ at 700 °C. The calculated lattice constants of $Sr_2Bi_2O_5$ calcined at 700 °C were a = 0.3825(3), b = 1.4282(9), and c = 0.6175(3) nm, which agree well with reference values [20]. There have been many reports on synthesis of $Sr_2Bi_2O_5$ by various methods. The formation temperature of $Sr_2Bi_2O_5$ phase depends on the preparation method; however, above 780 °C is necessary to form the $Sr_2Bi_2O_5$ phase in solid-state reactions. Additionally, calcination is usually repeated at higher temperature to obtain single-phase $Sr_2Bi_2O_5$ using conventional methods. Compared to the solid-state reaction, the present method could lower the formation temperature of $Sr_2Bi_2O_5$ by using a bimetallic complex precursor. The lower calcination temperature required to form $Sr_2Bi_2O_5$ from the bimetallic complex precursor relative to that needed in solid-state reaction is an advantage for practical applications.

The La-substituted DTPA complexes were calcined at 700 °C for 6 h in air and

compared with the obtained single phase of $Sr_2Bi_2O_5$ (Fig. 4(b)). No traces of impurity phases were detected in the 3 and 5 mol% La-doped $Sr_2Bi_2O_5$ powders. Meanwhile, the powders containing 8 and 10 mol% La contained a mixture of phases including $Sr_5Bi_6O_{14}$, $SrCO_3$, and $Sr_2Bi_2O_5$. These results suggest that the solubility limit of La atoms in $Sr_2Bi_2O_5$ is less than 8 mol%. The diffraction peaks for 3 and 5 mol% La-doped $Sr_2Bi_2O_5$ were not shifted from those of the undoped $Sr_2Bi_2O_5$ phase, mainly because of the similar ionic radii of La^{3+} and Bi^{3+}. However, there is an apparent doping limitation of La. This might be a lower tolerance crystal structure originated from the distorted local structure of $[BiO_6]$ polyhedra.

The mean crystallite size and BET specific surface area for the La-doped and undoped $Sr_2Bi_2O_5$ powders were evaluated. The mean crystallite sizes of the samples were calculated from the full width at half-maximum (FWHM) of the (111) diffraction peak at $2\theta = 28.11°$ using the Scherrer equation:

$$d = 0.9\lambda/B\cos\theta, \qquad \text{(equation 1)}$$

where λ is the wavelength of $CuK\alpha_1$ radiation, B is the FWHM of the (111) diffraction peak, θ is the Bragg angle, and d is the crystallite size. After calcination at 700 °C in air, the crystallite sizes of the undoped, and 5 and 10 mol% La-doped $Sr_2Bi_2O_5$ were estimated to be 47.2, 49.1, and 49.1 nm, respectively. The BET specific surface area of the undoped $Sr_2Bi_2O_5$ powder was calculated to be 3.9 m^2/g by applying the least-squares method to the BET plot. Doping $Sr_2Bi_2O_5$ with La caused the BET surface area to gradually increase with the amount of La, with BET specific surface areas of 4.4 m^2/g and 4.7 m^2/g for 5 and 10 mol% La-doped $Sr_2Bi_2O_5$, respectively. However, there were no notable changes in surface areas upon La doping. This suggests that La doping hardly affected the grain growth behavior of $Sr_2Bi_2O_5$ at 700 °C.

3.3. SEM and TEM observation

Figure 5 presents SEM images of the La-doped and undoped powders calcined at 700 °C. The undoped $Sr_2Bi_2O_5$ powder consists of tightly interconnected irregular grains. When 5 mol% La was added to $Sr_2Bi_2O_5$, gaps between the primary particles could be observed. Meanwhile, 10 mol% La-doped $Sr_2Bi_2O_5$ consisted of individual fine particles with diameters of 0.2–0.4 μm. These changes in microstructure are consistent with the slight increase in BET specific surface area induced by doping with

La. A typical HRTEM image of undoped $Sr_2Bi_2O_5$ (Fig. 5(d)) revealed well-crystallized particles with clear crystal lattices. No amorphous layer was observed along the surface or grain boundary of the crystallites. The crystalline planes were ascribed to the (002) and (131) planes of $Sr_2Bi_2O_5$ by considering the bond distances and arrangement of atoms in this image. HRTEM images of 5 and 10 mol% La-doped $Sr_2Bi_2O_5$ are depicted in Fig. 5(e) and (f), respectively. The contours of the observed crystalline planes were fairly clear and they were not covered by amorphous phases. These images suggest that $Sr_2Bi_2O_5$ could be doped with La without inducing formation of amorphous phases.

3.4. XRF, XPS and Raman spectroscopy

XRF analysis indicated that the content of La in 5 and 10 mol% La-doped $Sr_2Bi_2O_5$ were 4.9 and 12.2 mol%, respectively. The spectra of O 1s, Sr 3d, Bi 4f, and La 3d for 10 mol% La-doped $Sr_2Bi_2O_5$ obtained by XPS measurements are compared with those for undoped $Sr_2Bi_2O_5$ in Fig. 6. Peaks were corrected related to the C 1s signal centered at 285.0 eV. The O 1s spectrum of undoped $Sr_2Bi_2O_5$ contained two components at 529.0 and 530.8 eV. The former corresponds to lattice oxygen, while the latter originates from carbonate formed at the surface of $Sr_2Bi_2O_5$ [21]. The binding energies of the Sr 3d, Bi 4f and La 3d signals are in good agreement with those of the Sr^{2+}, Bi^{3+}, and La^{3+} valence states [22–24]. Although a La 3d signal was detected for 10 mol% La-doped $Sr_2Bi_2O_5$, it was difficult to clearly distinguish the La 3d signal from the background for 5 mol% La-doped $Sr_2Bi_2O_5$, which may be because the overall atomic concentration of La in this sample was relatively low.

Figure 7 depicts Raman spectra of the undoped and La-doped $Sr_2Bi_2O_5$ samples. The spectrum of the undoped powder contained sharp peaks at approximately 129 and 141 cm^{-1}, which were ascribed to $Sr_2Bi_2O_5$ according to Zhang *et al* [25]. The spectrum of undoped $Sr_2Bi_2O_5$ also contained broad peaks at 277, 320, 382, 416, 465, 549, and 647 cm^{-1}. According to the literature [25], the shift below 400 cm^{-1} is related to Bi-O bonds, and the two peaks centered at 549 and 647 cm^{-1} are related to Sr-O bonds. It is conceivable that other two peaks between 400 and 500 cm^{-1} are originated from Bi-O bonds because α-Bi_2O_3 has also the Raman peaks in same range [26]. However, until recently the Raman study on $Sr_2Bi_2O_5$ has been the subject of only a limited number of reports. Thus, further detailed investigations of Raman spectra are required to confirm

the present presumption. The mode centered at 1070 cm^{-1} is attributed to the A_{1g} mode of $SrCO_3$ [27]. When 5 mol% La atoms were doped into $Sr_2Bi_2O_5$, the intensity of the broad modes in the range of 277 to 465 cm^{-1} increased. Raman spectra become broad when lattice defects are introduced into a crystal because of the breaking of the selection rule for the wave vector. As expected, the stereochemically active lone pair (Bi 6s electrons) is strongly associated with electrons of the oxygen atoms surrounding Bi^{3+}. Thus, Bi^{3+} tends to shift from a centrosymmetric site to one with lower symmetry, thereby lowering its symmetry and coordination number [28]. Therefore, the local coordination environment of Bi^{3+} is highly asymmetric. Table 1 shows bond length obtained from the structure-optimized calculations for La-doped supercells using CASTEP code. La^{3+} has a similar ionic radius to Bi^{3+} but has no lone pair electrons. Thus, the Bi (or La) centered coordination polyhedron becomes more symmetrical structure by La doping judging from the bonding distances listed in Table1. Thus, the increase in the intensity of Raman peaks in the range of 277 to 465 cm^{-1} originates from Bi atoms being substituted with La atoms. For the Raman peaks below 446 cm^{-1}, there is no distinct difference between the samples containing 5 and 10 mol% La, as illustrated in Fig. 7. However, the intensity of the Raman peak centered at 614 cm^{-1} increased with the content of La, suggesting that La atoms substitute not only Bi atoms but also Sr atoms in 10 mol% La-doped $Sr_2Bi_2O_5$.

3.5. Diffused reflectance UV-vis spectra

UV-vis DRS for the samples calcined at 700 °C were collected in the wavelength range of 300 to 800 nm at room temperature. Figure 8 compares the spectral dependence of the Kubelka-Munk (KM) function defined by $f(R_\infty) = (1-R_\infty)^2/2R_\infty$, where R_∞ is the diffuse reflectance of the undoped $Sr_2Bi_2O_5$ prepared from the DTPA complex. The KM function $f(R_\infty)$ for the semi-infinite case is given by $f(R_\infty) = \alpha/S$ [29], where α and S are the absorption coefficient and scattering coefficient of the sample, respectively. Here, α was determined by [30]:

$$\alpha = A(h\nu - E_g)^n/h\nu, \qquad \text{(equation 2)}$$

where A, $h\nu$ and E_g are a constant, the photon energy and optical band gap of the sample, respectively. In equation 2, n depends on the nature of the band transition; n = 1/2 for direct and n = 2 for indirect allowed transitions. For the $Sr_2Bi_2O_5$ powder calcined at

700 °C, n was estimated to be 1/2 from the slope of a plot of $ln\ f(R_\infty)h\nu$ against $ln\ (h\nu\text{-}E_g)^n$ plot, suggesting that $Sr_2Bi_2O_5$ has a direct band gap. This result is consistent with a first-principles energy-band calculation for $Sr_2Bi_2O_5$ based on GGA and MBJ-LDA approaches [9,10]. Notably, as the content of La^{3+} increases, the absorption edge exhibits a red shift from that of undoped $Sr_2Bi_2O_5$. The magnitude of this shift increased with La^{3+} content; *i.e.*, the band gap of the samples decreases with increasing La^{3+} content. The band gaps of undoped, and 5 and 10 mol% La-doped $Sr_2Bi_2O_5$ samples were 3.2, 2.7, and 2.5 eV, respectively, according to respective plots of $\{f(R_\infty)h\nu\}^2$ *vs*. $h\nu$.

3.6. First-principles band calculation

To investigate the band structure, we carried out the first-principle band calculation using La-doped $Sr_2Bi_2O_5$ supercells (type 1 and 2). Figure 9 shows the total density of states and La-related DOS for La-doped and undoped $Sr_2Bi_2O_5$ obtained from the GGA calculation. The energy was measured in electron volts (eV) and the origin of energy was arbitrarily set as the VB maximum. It is well known that the GGA calculation underestimates the energy gaps of semiconductors and insulators, because the self-interaction correction and discontinuity in the exchange-correlation energy and potential upon changing the number of electrons are not taken into account [31, 32]. Although the underestimation of band gap energy might be included, the order of calculated band-gaps for three crystal phase of TiO_2, rutile, anatase, and brookite, conforms well to the order of optical band gaps [33]. Therefore, it is possible to compare the difference of band-gap difference between La-doped and undoped $Sr_2Bi_2O_5$ qualitatively in the framework of the GGA.

For undoped $Sr_2Bi_2O_5$, the VB is constructed from O 2p, Bi 6s, Bi 6p, Sr 4p, and Sr 4d states; however, the character of O 2p states is predominant [9]. In addition, the CB below 4.3 eV mainly consists of Bi 6p and O 2p states. Although the VB and CB structures of $Sr_2Bi_2O_5$ are slightly altered by replacing one Bi atom with one La atom, of particular interest is that the band gap of $Sr_2Bi_2O_5$ decreases by approximately 0.1 eV upon La addition compared with that of undoped $Sr_2Bi_2O_5$. Such change of band gap with the addition of a rare-earth dopant is strange because the band gap is an intrinsic feature of the host material, and the concentration of doped La is very low. However,

this decrease of band gap was also observed in the UV-vis spectra of the La-doped $Sr_2Bi_2O_5$ samples, as mentioned above. One plausible explanation for this may be derived from the difference in the number of oxygen atoms that coordinate with Bi or La atoms. As stated above, Bi^{3+} possesses a stereochemically active lone pair (Bi 6s electrons), and this electron pair is strongly associated with the electrons of oxygen atoms surrounding Bi^{3+}. The ionic radius of La^{3+} is similar to that of Bi^{3+} but it has no lone pair electrons. The introduction of La^{3+} into the lattice makes the coordination polyhedron more symmetric as observed in Table 1. This change in the coordination environment of La^{3+} is expected to weaken the repulsive interaction between the lone pair electron and oxygen compared with the case before substitution with La^{3+}. Therefore, it is conceivable that the band gap of $Sr_2Bi_2O_5$ is lowered by substituting Bi^{3+} with La^{3+}.

3.7. Photocatalytic properties

Figure 10 shows CO_2 concentration as a function of irradiation time for the oxidation of isopropanol by the undoped and La-doped $Sr_2Bi_2O_5$ samples. As a comparison, isopropanol oxidation over commercially available TiO_2 (Degussa P-25, 48.0 m^2/g) was also carried out under the same conditions. Only a small amount of CO_2 was generated following visible-light irradiation of TiO_2 and undoped $Sr_2Bi_2O_5$. In contrast, La-doped $Sr_2Bi_2O_5$ samples caused a considerable increase in CO_2 concentration. The oxidation of isopropanol is apparently accelerated by La-doped samples, suggesting they possess higher photocatalytic activities than those of TiO_2 and undoped $Sr_2Bi_2O_5$. The results also revealed that an increased content of La in $Sr_2Bi_2O_5$ caused the amount of generated CO_2 to increase. This is mainly related to the red shift of the photoabsorption of the La-doped samples as La content increases; however, the quantum efficiency of the samples remains to be investigated. The chemical stability of the La-doped and undoped $Sr_2Bi_2O_5$ samples was investigated by XPS, UV-vis spectroscopy and XRD after the photocatalytic activity measurements. We concluded that the La-doped and undoped $Sr_2Bi_2O_5$ samples possessed sufficient stability judging from their unchanged XRD profiles. However, the formation of $SrCO_3$ and $La_2(CO_3)_3$ on the surface of the samples was detected, so the long-term stability and sustainability of the photocatalytic activity of the samples requires further study. Although 10 mol%

La-doped $Sr_2Bi_2O_5$ showed the highest photocatalytic activity among the samples tested here.

4. Conclusion

Undoped and La-doped $Sr_2Bi_2O_5$ samples were fabricated by calcination of heterobimetallic complex Sr[Bi(DTPA)]•$9H_2O$ at 700 °C, and the precursor complex and calcined samples were characterized by various techniques. Single-phase $Sr_2Bi_2O_5$ was formed after calcination of Sr[Bi(DTPA)]•$9H_2O$ at a rather lower temperature of 700 °C for 6 h in air. For the La-doped samples, no impurity phases were observed in the samples with 3 and 5 mol% La, whereas impurity phases such as $Sr_3Bi_4O_8$ and $SrCO_3$ were detected in the samples containing 8 and 10 mol% La. The BET surface area of the $Sr_2Bi_2O_5$ samples increased slightly with La content. SEM observation revealed that the $Sr_2Bi_2O_5$ samples consisted of tightly interconnected grains and that the open pores between particles tended to increase with La content. HRTEM observation showed clear crystalline planes for both undoped and La-doped $Sr_2Bi_2O_5$ without amorphous phases. In XPS measurements of the La-doped and undoped $Sr_2Bi_2O_5$, the binding energies of the Sr 3d, Bi 4f, and La 3d signals were consistent with the Sr^{2+}, Bi^{3+}, and La^{3+} valence states, respectively. The Raman scattering measurements suggested that La atoms were located at Bi sites with the doping amount of La was low (3 and 5 mol%), whereas La atoms tended to substitute both Bi and Sr sites with the content of La was higher (8 and 10 mol%). XRD and Raman scattering results strongly indicated that the solubility limit of La in $Sr_2Bi_2O_5$ is below 8 mol%. La-doped $Sr_2Bi_2O_5$ exhibited a red shift of its absorption edge as the content of La increased, reaching the visible region. Optimized structure calculations based on the DFT method revealed that the coordination number of oxygen atoms surrounding the Bi^{3+}-site increases upon substituting with La^{3+}. Furthermore, the DOS calculation reproduced the band-gap narrowing of $Sr_2Bi_2O_5$ upon La addition observed in UV-vis spectra. Preliminary catalytic experiments indicated that the photocatalytic activity of $Sr_2Bi_2O_5$ under visible-light irradiation can be enhanced by doping with La.

References

[1] H. Maeda, T. Tanaka, M. Fukutomi, T. Asano, A new high-T_c oxide superconductor without a rare earth element, Jpn. J. Appl. Phys. 27 (1988) L209.

[2] K.T. Jacob, K.P. Jayadevan, System Bi–Sr–O: synergistic measurements of thermodynamic properties using oxide and fluoride solid electrolytes, J. Mater. Res. 13 (1998) 1905.

[3] Z. Shan, Y. Xia, Y. Yang, H. Ding, F. Huang, Preparation and photocatalytic activity of novel efficient photocatalyst $Sr_2Bi_2O_5$, Mater. Lett. 63 (2009) 75.

[4] Y. Obukuro, K. Obata, S. Matsushima, M. Arai, K. Kobayashi, Preparation and characterization of SrO-Bi_2O_3 complex oxide, Funct. Mater. Lett. 5 (2012) 260015-1.

[5] E. Asato, K. Kamamuta, R. Imade, M. Yamasaki, Solution structures and ligand exchange dynamics of bismuth (III) complexes with nitrilotriacetic acid and N-(2-hydroxyethyl) iminodiacetic acid**,** Inorg. React. Mech. 2 (2000) 57.

[6] M. Sakamoto, P. Nunziante, E. Traversa, S. Matsushima, M. Miwa, H. Aono, Y. Sadaoka, Preparation of perovskite-type oxides by the thermal decomposition of heteronuclear complexes, $Ln[Fe_xCo_{1-x}(CN)_6]\cdot 4H_2O$ (Ln = Pr-Yb), J. Ceram. Soc. Jpn. 105 (1997) 963.

[7] Y. Obukuro, G. Sakai, Y. Okuyama, N. Matsunaga, S. Matsushima, K. Obata, E. Asato, Preparation and characterization of heterobimetallic complex, $Sr[Bi(DTPA)]\cdot 9H_2O$, derived La-doped $Sr_2Bi_2O_5$, Chem. Lett. (2015) DOI: 10.1246/cl.150178.

[8] M. Kohno, S. Ogura, S. Sato, Y. Inoue, Properties of photocatalysts with tunnel structures: formation of a surface lattice O^- radical by the UV irradiation of $BaTi_4O_9$ with a pentagonal-prism tunnel structure, Chem. Phys. Lett. 267 (1997) 72.

[9] Y. Obukuro, H. Nakamura, K. Obata, S. Matsushima, M. Arai, K. Kobayashi, First-principles study on electronic structure of $Sr_2Bi_2O_5$ crystal, J. Phys. Chem. Solids 72 (2011) 1477.

[10] Y. Obukuro, S. Matsushima, K. Obata, M. Arai, K. Kobayashi, Improved calculation of band gap of $Sr_2Bi_2O_5$ crystal using modified Becke–Johnson exchange potential, J. Phys. Chem. Solids 75 (2014) 427.

[11] S. Barunauer, L.S. Deming, W.E. Deming, E.J. Teller, On a theory of the van der Waals adsorption of gases, J. Am. Chem. Soc. 62 (1940) 1723.

[12] S. Barunauer, P.H. Emmet, E. Teller, Adsorption of gases in multimolecular layers, J. Am. Chem. Soc. 60 (1938) 309.

[13] C.C. Torardi, J.B. Parise, A. Santoro, C.J. Rawn, R.S. Roth, B.P. Burton, $Sr_2Bi_2O_5$: A structure containing only 3-coordinated bismuth, J. Solid State Chem. 93 (1991) 228.

[14] V. Milman, B. Winkler, J. A. White, C. J. Pickard, M.C. Payne, E.V. Akhmatskaya, R.H. Nobes, Electronic structure, properties, and phase stability of inorganic crystals: A pseudopotential plane-wave study, Int. J. Quantum Chem. 77 (2000) 895.

[15] J.P. Perdew, K. Burke, M. Ernzerhof, Generalized gradient approximation made simple, Phys. Rev. Lett. 77 (1996) 3865.

[16] D. Vanderbilt, Soft self-consistent pseudopotentials in a generalized eigenvalue formalism, Phys. Rev. B41 (1990) 7892.

[17] H.J. Monkhorst, J.D. Pack, Special points for Brillouin-zone integrations, Phys. Rev. B13 (1976) 5188.

[18] P. Blaha, K. Schwarz, G. K. H. Madsen, D. Kvasnicka, J. Luitz, WIEN2k, An Augmented Plane Wave + Local Orbitals Program for Calculating Crystal Properties (Karlheinz Schwarz, Techn. Universitat Wien, Austria, 2001).

[19] K. Nakamoto, in Infrared and Raman Spectra of Inorganic and Coordination Compounds, 3rd edn, J. Wiley, New York, 1978.

[20] J.F. Vente, R.B. Helmholdt and D.J.W. Ijdo, Structure of $Sr_2Bi_2O_5$ from X-ray and neutron powder diffraction data, Acta Crystallogr. C 48 (1992) 1380.

[21] F. Voigts, F. Bebensee, S. Dahle, K. Volgmann, W. Maus-Friedrichs, The adsorption of CO_2 and CO on Ca and CaO films studied with MIES, UPS and XPS, Surf. Sci. 603 (2009) 40.

[22] E.J. Crumlin, E. Mutoro, W.T. Hong, M.D. Biegalski, H.M. Christen, Z. Liu, H. Bluhm, Y.Shao-Horn, In situ ambient pressure X-ray photoelectron spectroscopy of cobalt perovskite surfaces under cathodic polarization at high temperatures, J. Phys. Chem. C 117 (2013) 16087.

[23] Z.P. Gao, H.X. Yan, H.P. Ning, R. Wilson, X.Y. Wei, B. Shi, H. Ye, M.J. Reece, Piezoelectric and dielectric properties of Ce substituted $La_2Ti_2O_7$ ceramics, J. Europ. Ceram. Soc. 33 (2013) 1001.

[24] H.W. Kang, S.N. Lim, S.B. Park, Organic-inorganic composite of g-C_3N_4–$SrTiO_3$:Rh photocatalyst for improved H_2 evolution under visible light irradiation, Int. J. Hydrogen Energy 37 (2012) 4026.

[25] F.X. Zhang, B. Manoun, S.K. Saxena, C.S. Zha, Structural changes of Na_xCoO_2 (x=0.74) at high pressures, J. Solid State Chem. 179 (2006) 544.

[26] Y. Wang, Y. He, T. Li, J. Cai, M. Luo, L. Zhao, Photocatalytic degradation of methylene blue on $CaBi_6O_{10}/Bi_2O_3$ composites under visible light, Chem. Eng. J, 189 (2012) 473.

[27] S. Ni, X. Yang, T. Li, Hydrothermal synthesis and photoluminescence properties of $SrCO_3$, Mater. Lett. 65 (2011) 766.

[28] F.N. Sayed, V. Grover, B.P. Mandal, A.K. Tyagi, Influence of La^{3+} substitution on electrical and photocatalytic behavior of complex $Bi_2Sn_2O_7$ oxides, J. Phys. Chem. C 117 (2013) 10929.

[29] P. Kubelka, New contributions to the optics of intensely light-scattering materials. part I, J. Opt. Soc. Am. A 38 (1948) 448.

[30] H. Demirryont, J.R. Sites, Effects of oxygen in ion-beam sputter deposition of titanium oxides, J. Vac. Sci. Technol. A 2 (1984) 1457.

[31] R.O. Jones, O. Gunnarsson, The density functional formalism, its applications and prospects, Rev. Mod. Phys. 61 (1989) 689.

[32] P. Mori-Sanchez, A.J. Cohen, W.T. Yang, Localization and delocalization errors in density functional theory and implications for band-gap prediction, Phys. Rev. Lett. 100 (2008) 146401.

[33] S. Matsushima, K. Obata, H. Yamane, K. Yamada, H. Nakamura, M. Arai, K. Kobayashi, First-principles band calculation of TiO_2 with brookite structure, Electrochem., 72 (2004) 694.

Figure caption

Fig. 1. (color online) Unit cell and La-doped $Sr_2Bi_2O_5$ supercells used in the theoretical calculation. La (sky blue), Bi (purple), Sr (green), O (red).

Fig. 2. IR spectra of metal-free H_5DTPA and Sr[Bi(DTPA)]•$9H_2O$.

Fig. 3. TG and DTA curves for Sr[Bi(DTPA)]·$9H_2O$.

Fig. 4. (color online) XRD patterns of the calcined sample powders by (a) Sr[Bi(DTPA)]•$9H_2O$ at 500 to 700 °C for 6 h and (b) La-doped DTPA complexes at 700 °C.

Fig. 5. SEM images of (a) Undoped, (b) 5 mol%, and (c) 10 mol% La-doped powders and TEM photographs of (d) Undoped, (e) 5 mol%, and (f) 10 mol% La-doped powders calcined at 700 °C.

Fig. 6. (color online) XPS spectra of O 1s, Sr 3d, Bi 4f, and La 3d for 10 mol% La-doped (solid line) and undoped $Sr_2Bi_2O_5$ (dotted line).

Fig. 7. (color online) Raman spectra obtained for La-doped and pure $Sr_2Bi_2O_5$ powders.

Fig. 8. (color online) UV-vis DRS for La-doped and pure $Sr_2Bi_2O_5$ powders obtained by the calcination at 700 ^{o}C in air for 6 h.

Fig. 9. (color online) Total and partial DOS for (a) undoped (unit cell) and La-doped $Sr_2Bi_2O_5$ supercell, (b) type 1 and (c) type 2, obtained from the GGA calculation.

Fig. 10. (color online) Time-dependent profiles of isopropanol decomposition and CO_2 generation over photocatalysts under visible-light irradiation.

Table 1 Calculated bond distances of $Sr_2Bi_2O_5$ and La-doped $Sr_2Bi_2O_5$ by CASTEP.

Unit cell	Distance / nm	Type 1	Distance / nm
Bi1-O2 (×2)	0.2119	La1-O17 (×2)	0.2141
Bi1-O1	0.2197	La1-O39	0.2299
Bi1-Sr1	0.3654	La1-O26 (×2)	0.3514
Bi1-Bi2 (×2)	0.3657	La1-Bi6 (×2)	0.3647
Bi1-O3 (×2)	0.3691	La1-Sr15	0.3689
Unit cell	Distance / nm	Type 2	Distance / nm
Bi2-O3 (×2)	0.2123	La2-O26 (×2)	0.2147
Bi2-O1	0.2186	La2-O39	0.2276
Bi2-Sr2	0.3543	La2-O9 (×2)	0.3494
Bi1-Bi2 (×2)	0.3657	La2-Sr12	0.3585
Bi2-O2 (×2)	0.3672	La2-Bi3 (×2)	0.3653

Fig. 1

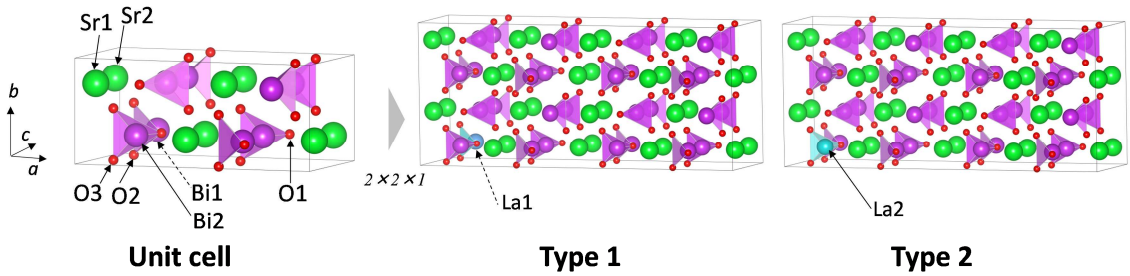

Fig. 2

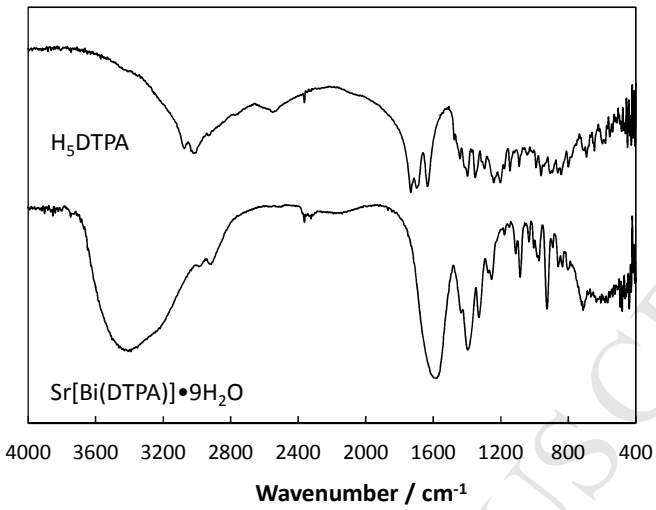

Fig. 3

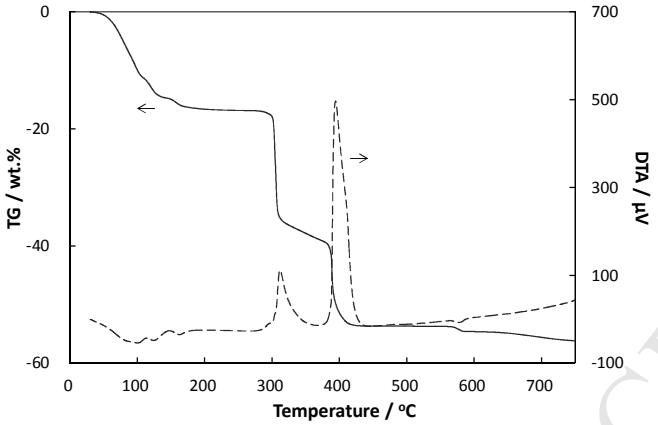

Fig. 4

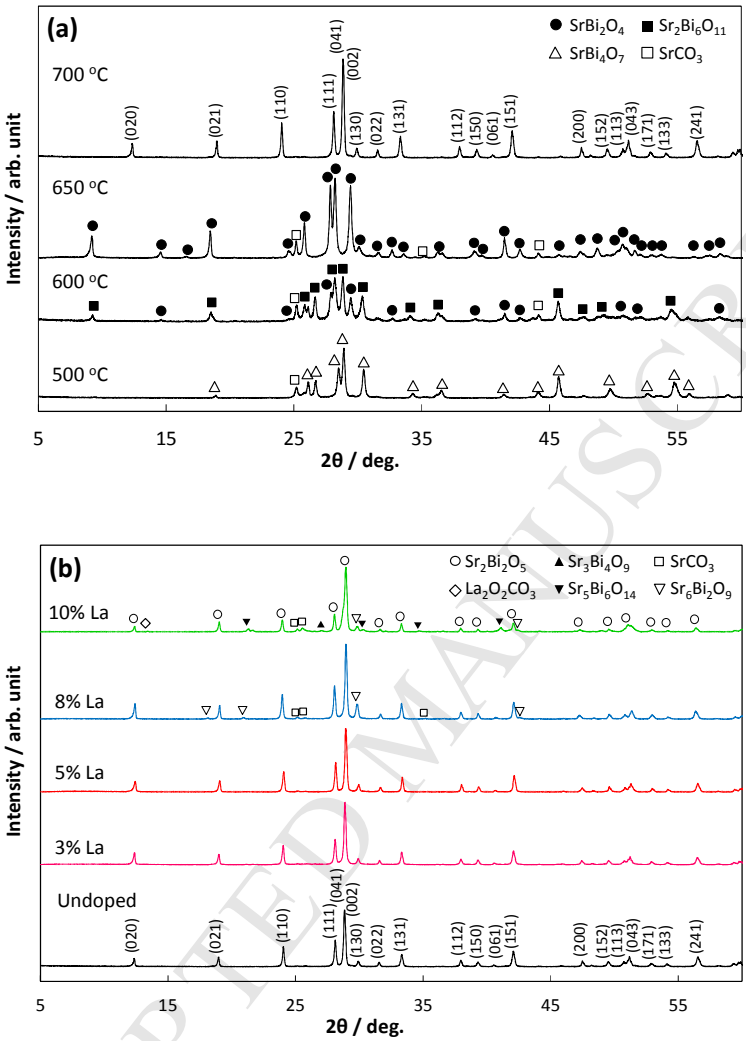

Fig. 5

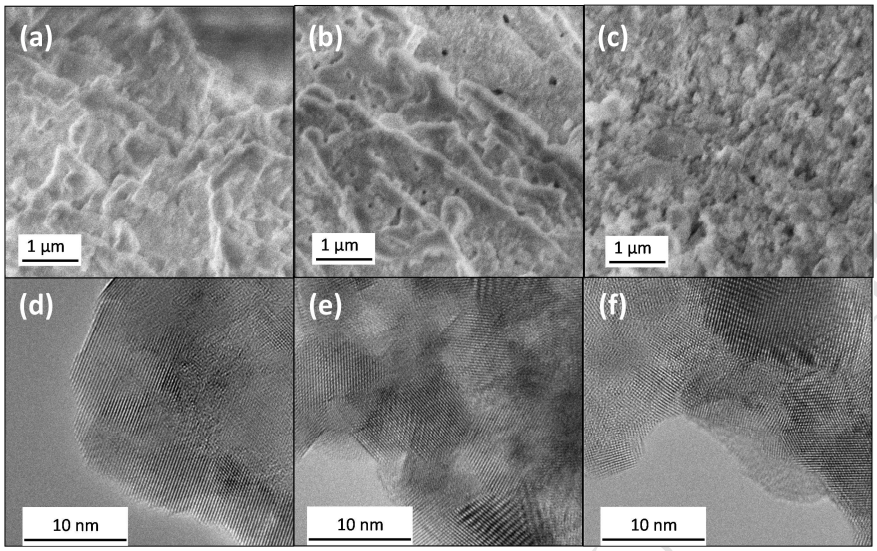

Fig. 6

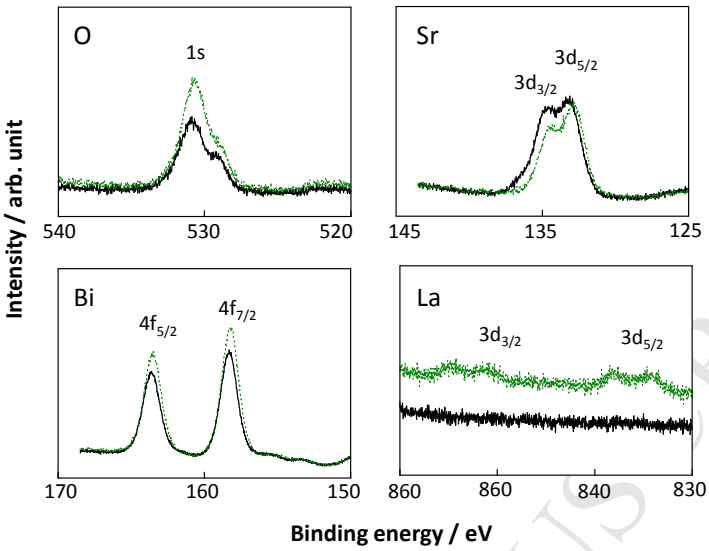

Fig. 7

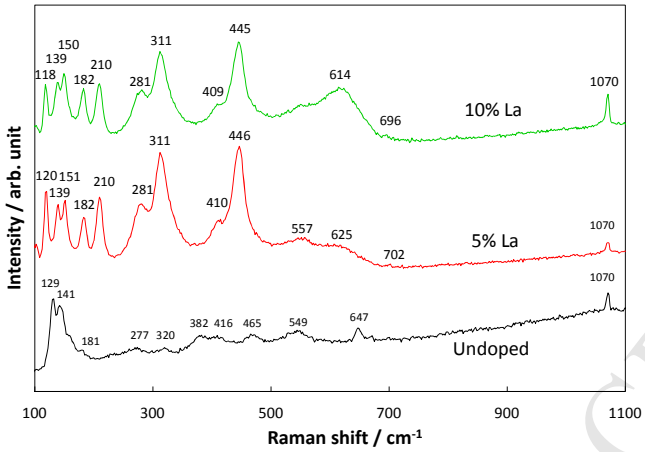

Fig. 8

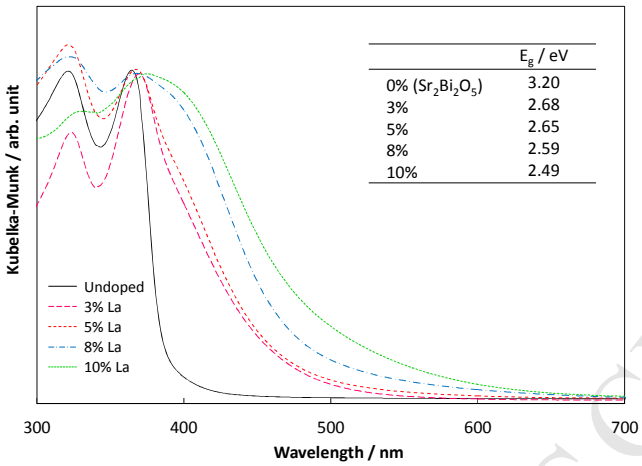

Fig. 9

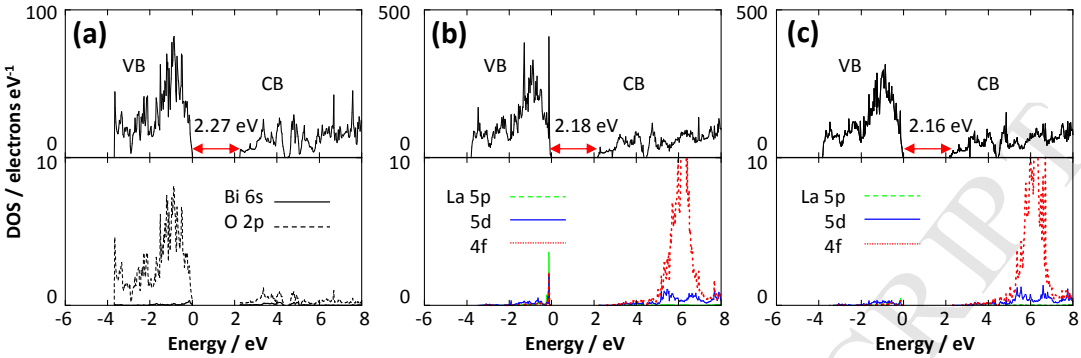

Fig. 10

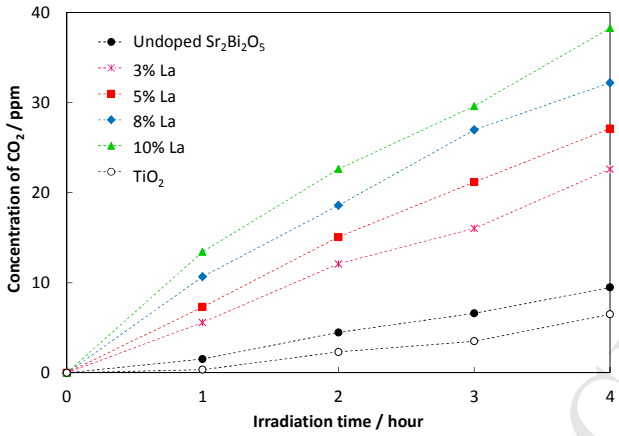

- La-doping showed a red shift of absorption, reaching the visible region.
- La-doping increased the coordination number of oxygen surrounding the Bi^{3+}-site.
- The energy band calculations showed the band gap narrowing by La-doping.
- A superior photocatalytic performance was observed under visible-light.